REPORT DOCUMENTATION PAGE

Form Approved
OMB No. 0704-0188

PLEASE DO NOT RETURN YOUR FORM TO THE ABOVE ORGANIZATION.

1. REPORT DATE *(DD-MM-YYYY)*	2. REPORT TYPE	3. DATES COVERED *(From - To)*
14-12-2010	Final	Sep 2006 - Aug 2010; Dec 2010

4. TITLE AND SUBTITLE
Lattice-Engineered Materials and Vertically-Integrated Multijunctions for Multi-Spectral Photodetectors

5a. CONTRACT NUMBER

5b. GRANT NUMBER
FA9550-06-1-0557

5c. PROGRAM ELEMENT NUMBER

6. AUTHOR(S)
Ringel, Steven, A.

5d. PROJECT NUMBER

5e. TASK NUMBER

5f. WORK UNIT NUMBER

7. PERFORMING ORGANIZATION NAME(S) AND ADDRESS(ES)
The Ohio State University
Department of Electrical and Computer Engineering
2015 Neil Avenue
Columbus, OH 43210

8. PERFORMING ORGANIZATION REPORT NUMBER

9. SPONSORING/MONITORING AGENCY NAME(S) AND ADDRESS(ES)
Air Force Office of Scientific Research
875 N. Randolph Street
Arlington Virginia, 22203

10. SPONSOR/MONITOR'S ACRONYM(S)
AFOSR

11. SPONSOR/MONITOR'S REPORT NUMBER(S)
AFRL-OSR-VA-TR-2012-0168

12. DISTRIBUTION/AVAILABILITY STATEMENT
Approved for public release; distribution unlimited.

13. SUPPLEMENTARY NOTES

14. ABSTRACT
This final report describes recently achieved advances in integrating infrared and visible band III-V compound photodetectors to create a monolithic, vertically-integrated, high performance multispectral photodetector device in which multiple wavelength bands can be detected and distinguished simultaneously, without need for external bias control. To accomplish this new device architecture, novel heterostructures were designed and realized that utilize bandgap engineering to tune the sub-detector bandgaps and energy band offsets, coupled with substrate engineering via metamorphic grading of the lattice constant to control defect formation, within the InGaP-InGaAs materials systems. Specific novelties include the development of internal current blocking isolation layers so that a three-terminal configuration could be utilized and development of a novel overshoot and step-back layer to optimize strain relaxation within the lattice-mismatched device layers. The approach developed in this effort defines a rational materials path for future compact, high performance multispectral detectors based on material systems with tunable optical properties on a single substrate.

15. SUBJECT TERMS
III-V Photodetector, Metamorphic Epitaxy, InGaAs, InGaP, Multispectral Detector, Monolithic Integration, Multijunction, Molecular Beam Epitaxy, Infrared and Visible Photodetectors

16. SECURITY CLASSIFICATION OF:			17. LIMITATION OF ABSTRACT	18. NUMBER OF PAGES	19a. NAME OF RESPONSIBLE PERSON
a. REPORT	b. ABSTRACT	c. THIS PAGE			Jo Ellen Scherrer
U	U	U	UU	19	19b. TELEPHONE NUMBER *(Include area code)* 614-292-5277

Electronic Materials and Devices Laboratory
Department of Electrical Engineering

Dr. Steven A. Ringel
Neal Smith Chair Professor
Dept. Electrical Engineering
The Ohio State University
2015 Neil Ave.
Columbus, Oh 43210-1272

Tel: (614) 292-6904
Fax: (614) 292-9562
ringel.5@osu.edu

Final Report

Lattice-Engineered Materials and Vertically-Integrated Multijunctions for Multi-Spectral Photodetectors

AFOSR Grant # FA9550-06-1-0557

PI: Professor Steven A. Ringel
Department of Electrical and Computer Engineering
The Ohio State University
2015 Neil Ave.
Columbus,OH 43210
(614) 292-6904 (ph)
(614) 292-9562 (fax)
ringel.5@osu.edu

Technical Monitor: Dr. Kitt Reinhardt
AFOSR/NE
875 Randolph Street Suite 325, Room 3112
Arlington, VA 22203
Kitt.Reinhardt@afosr.af.mil
Tel: (703) 588-0194

Contract Information

Grant Number	FA9550-06-1-0557
Title of Project	Lattice-Engineered Materials and Vertically-Integrated Multijunctions for Multi-Spectral Photodetectors
Principal Investigator	Steven A. Ringel
Organization	Department of Electrical and Computer Engineering The Ohio State University Columbus, OH 43210

1. Executive Summary

The objective of this research program was to explore the science and application of metamorphic III-V materials, combined with substrate engineering, leading to the creation of vertically-integrated multijunction detectors capable of selective band discrimination from the near infrared through the ultraviolet. The vertical structure eliminates the need for external optical control while also creating a compact design. The future goal enabled by this program is the development of multispectral detector stacks that independently operate in different wavelength bands without the need for active bias control, whose cutoffs can be designed through proper selection of bandgap profile as desired for specific applications. This program has focused on both the enabling materials science and the demonstration of prototype detectors based on novel device architectures. Multiple key issues in the critical path of this development were targeted and solved. These include development of low defect density, lattice mismatched III-V detector materials possessing a range of lattice constants needed for the target bandgaps, strategies for integrating metamorphic detectors of different bandgaps with "internal" lattice matching, and development of device and material heterostructure designs that achieve ideal electrical isolation and minimal out-of-band optical crosstalk for multispectral detectors. The materials system of choice used here is the AlGaInAsP III-V alloy system, and the effort therefore also focused on the necessary materials issues to enable high performance devices. A variety of metamorphic detectors were demonstrated based on InGaAs and InGaP, which showed extremely high performance by all detector metrics, and the first InGaP/InGaAs vertically integrated multijunction detector was achieved with superb electrical and optical isolation, under simultaneous operation. The project supported one PhD student and partially supported 2 other students and a postdoctoral researcher over the course of the effort, and resulted in eight journal publications in print to date, with three more pending, and a large number of conference presentations and invited talks.

2. General Scientific Approach

Since the main goal of this basic research effort is to create a materials platform that demonstrates the reality of vertically-integrated multispectral photo-detection schemes, tunable and optimizable with respect to mission-specific wavelength cutoffs and detection criteria, choice of material is critical. Conventionally, the issue of bulk bandgap selectively is constrained by the need to grow on a standard substrate platform, but our approach here is based on a virtual substrate approach, where the lattice constant and composition of the device-level materials can be designed such that the resultant absorption cutoff wavelengths of a vertically-stacked multi-band detector can be adjusted and optimized for specific applications (missions). Therefore, the choice of materials must both support optimum lattice grading (meaning the materials must have reasonably high dislocation glide velocities at growth temperature, controllable misfit nucleation, no phase separation issues, and reasonable match of thermal expansion coefficient) and simultaneously enable accessibility of the necessary range of bandgap energies.

Moreover, strong absorption above E_g is critical since the vertical structure necessitates that each sub-detector completely absorb its "band" of incident photons to maintain good contrast and out-of-band rejection, allowing only those photons with energies below the bandgap to pass through to the longer wavelength detector. Therefore, materials with direct bandgaps are necessary.

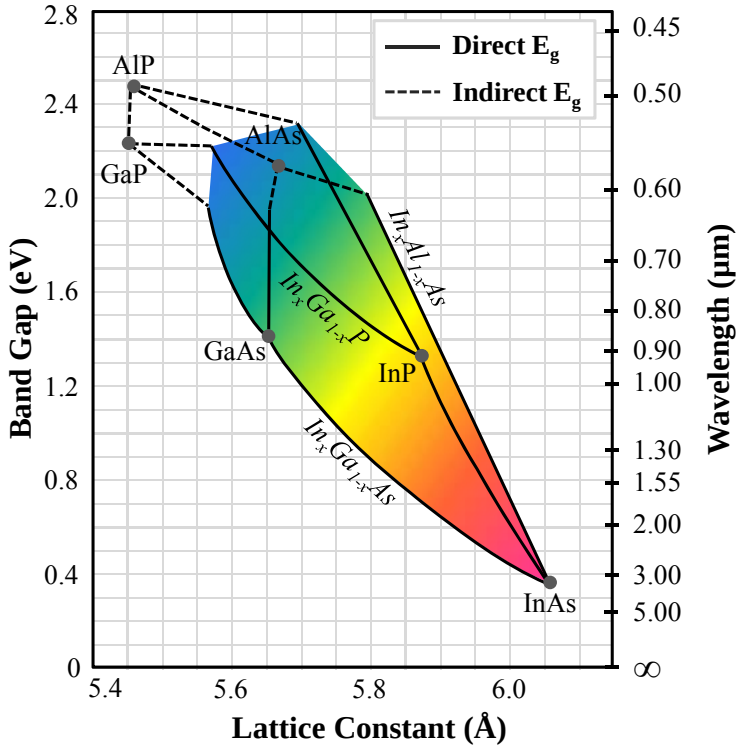

Figure 1. III-V compound semiconductor bandgap vs. lattice constant chart, with the shaded region indicating the potential range of useful compositions for multispectral photodetector applications.

Figure 1 gives the standard bandgap versus lattice constant chart for the typical III-AsP compound semiconductors, with the shaded region indicating the array of compositions providing absorption cutoffs (direct bandgaps) in the visible to mid-IR wavelength range. While there exists a large number of potentially useful alloy compositions in this range, there are restrictions in growing them in a straightforward manner due to the fact that there are a limited number of available substrate materials on which to perform the growth, with GaAs being the most robust and convenient. However, due to the large lattice constant mismatch between GaAs and any material compositions of interest and the resultant strain-induced relaxation of the mismatched epilayer by the nucleation and glide of dislocations, direct heteroepitaxial growth of such materials results in a high density of detrimental defects (dislocations), which severely degrades device performance. Therefore, our approach in this work is to utilize GaAs (a common substrate material) as the starting point for the growth of metamorphic (compositionally graded) buffers by molecular beam epitaxy (MBE). Such buffers allow for the careful control of the rate of strain introduction, and thus dislocation nucleation, during the growth, which with proper buffer design allows for the mitigation of even large degrees of lattice mismatch while maintaining an acceptably low dislocation density in the final device layers. While there are different methodologies that can be applied to the metamorphic buffer approach, we typically utilize compositional step-grading due to our ability to produce sharp, well-controlled heterointerfaces and compositions, providing for a high level of control over strain relaxation, and thus the evolution of the dislocation density, during the buffer growth.

In this work we have concentrated on target composition (and thus virtual substrates) with lattice constants larger than GaAs (compressively strained), thereby enabling the growth of materials with cutoff wavelengths in the near- and mid-IR, as well as in the long wavelength portion of the visible spectrum. The three most accessible alloy systems on which to conduct the necessary lattice constant and bandgap engineering are $In_xAl_{1-x}As$, $In_xGa_{1-x}As$, and $In_xGa_{1-x}P$. These alloys can also be grown internally lattice-matched to each other, enabling the growth of monolithic multi-detector device structures to achieve a multi-band absorption/detection profile at an arbitrary lattice constant. It is worth noting that it is also possible to move toward smaller lattice constants (tensile strained), and thus shorter wavelengths (visible), utilizing the $GaAs_yP_{1-y}$ and $In_xGa_{1-x}P$ alloy systems, but this is not within the scope of the work discussed herein.

For all of the work described in this report, we have utilized molecular beam epitaxy (MBE) as the method of materials growth. While MBE is not typically considered tractable for industrial-level production, it is an extremely useful research technique that provides a high level of control of the growth process, including growth temperatures, growth rates, and fluxes of reactant species. By defining the materials science via MBE, the basis for eventual MOCVD epitaxy can be developed; this has been a methodology we have employed with great success in other areas of lattice-mismatched heteroepitaxy for applications from photovoltaics to optoelectronics. The MBE grown samples are analyzed using a variety of techniques that give a wide range of materials properties. High-resolution triple-axis X-ray diffractometry (XRD) reciprocal space mapping (RSM) is used to characterize epilayer structural properties, including lattice constant (both lateral and vertical), as well as residual strain state (relaxation). Transmission electron microscopy (TEM) is used to provide a highly sensitive analysis of structural defects, including dislocations and phase decomposition. Fabricated devices structures (p-i-n photodetectors) also enable materials-related analysis, in addition to purely device-level properties, via a number of electronic and optoelectronic measurement techniques, including current-voltage (I-V) analysis, deep level transient spectroscopy (DLTS), and spectral response/quantum efficiency (QE), all of which can reveal information regarding potentially detrimental electronic defects and trap levels in the device epilayers. The fabricated devices are, of course, also analyzed for device-level properties, including detector spectral responsivity, capacitance-voltage (C-V), and noise equivalent power (NEP). While the specific details of the various measurements employed are not explicitly described in this report, the results are discussed in detail. *The resulting output of this program has not only led to the first such multi-spectral detectors reported, but the device characteristics of the devices out-perform standard commercial lattice-matched detector technologies available today, notwithstanding the additional novel advantage of multispectral behavior.*

3. Key Results and Discussion

Summary of major highlights:

- Demonstration of compressive overshoot and stepback layer approach to achieve optimal metamorphic InGaAs virtual substrates by MBE; ideal metamorphic substrates achieved for two target lattice constant-InGaAs compositions (14% and 20% In composition)
- 5 individual band p-i-n detector structures grown and fabricated with band cutoff wavelengths from ~1130 nm to ~660 nm achieved on same initial substrate
- Extraordinary low trap concentrations (10^{12} cm^{-3} range) in metamorphic InGaP and InGaAs equivalent to values in lattice-matched materials demonstrated; negligible effect of mismatch induced defects proven
- Prototype metamorphic single-junction IR (InGaAs) and visible photodetectors (InGaP and metamorphic InGaP) with record low leakage current and ideal photoresponse behavior
- First design, growth, fabrication and demonstration of monolithic vertically-integrated dual-band, metamorphic multijunction detectors that can be operated simultaneously and independently in multiple bands with ideal electrical isolation and strong out-of-band optical rejection
- Process and design is transferrable to 3-4 band designs, is transferrable to Si substrates, and is scalable on GaAs platforms

Description of selected highlights and results obtained:

3.1. Metamorphic Virtual Substrate Materials on GaAs

A. Choice of metamorphic alloy system

InAlAs, InGaP and InGaAs are the ternary grading materials systems available for accessing lattice constants larger than that of GaAs. For many metamorphic materials applications, including back-side illuminated photodetectors and inverted metamorphic solar cells, it is necessary to use a grading material with a wider bandgap to maintain effective "optical transparency" with respect to the terminal device layers. For this purpose, InAlAs and InGaP have been used extensively. However, issues related to the presence of Al in InAlAs (and other Al containing materials like InAlGaAs) tends reduce the efficacy of metamorphic grading, which can have adverse effects on device performance.

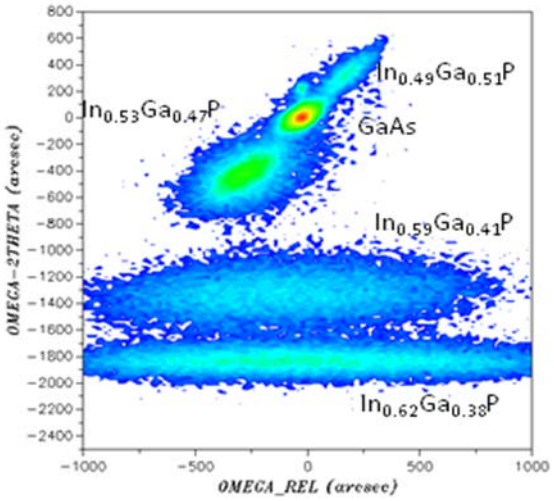

Figure 2. High-resolution TA-XRD RSM from the symmetric (004) reflection of a step-graded metamorphic $In_xGa_{1-x}P$ buffer structure grown on GaAs(100), accommodating a total 1% lattice misfit.

Metamorphic $In_xGa_{1-x}P$ step-graded buffers grown on GaAs substrates show extremely high XRD mosaicity, and thus low crystalline quality (see Figure 2). We have shown this to be a result of phase segregation of the metamorphic InGaP into In-rich and In-deficient areas due to bonding competition between In and Ga atoms as we move away from the lattice-matched composition of $In_{0.49}Ga_{0.51}P$ on GaAs. Also, from a practical standpoint, using InGaP as the grading material requires crossing over between As- and P-based growth regimes twice (for the growth of narrow bandgap InGaAs materials), which has the potential to negatively impact the quality of the interface, and possibly the overall device performance.

Therefore, InGaAs was chosen as the material for compositional grading used for this work. Of course, the metamorphic InGaAs system also has its challenges, and a fair amount of work was done to find the optimal growth conditions for the various compositions used for the metamorphic buffer.

B. Metamorphic InGaAs buffer structural analysis

To date, two different InGaAs virtual substrate compositions have been developed: $In_{0.14}Ga_{0.86}As$ and $In_{0.20}Ga_{0.80}As$. Optimum growth conditions were determined from analysis of in-situ reflection high energy-electron diffraction (RHEED), post-growth surface roughness observations from Nomarski optical microscopy and atomic force microscopy (AFM), and post-growth structural analysis by TA-XRD reciprocal space maps (RSM). A series of growth studies led us to determine a well controlled, optimal growth methodology in which a retrograde growth temperature profile was employed as a function of increasing In% during growth in the InGaAs graded buffer. Table 1 gives an example growth design for the specific case of $In_{0.14}Ga_{0.86}As$ virtual substrates, for which the substrate temperature was reduced from ~610°C for the initial GaAs layer to ~550°C and ~515°C, while increasing In% from 0% to 6% and 12%, respectively, followed by extension to 17% and 14% In content at the

Table 1. Growth process for the $In_{0.14}Ga_{0.86}As$ virtual substrate, including composition, misfit (with respect to GaAs), and growth temperature for each buffer layer.

Layer	%Misfit (wrt GaAs)	T_{sub} (°C)
GaAs	0.00	610
$In_{0.06}Ga_{0.94}As$	0.43	550
$In_{0.12}Ga_{0.88}As$	0.86	515
$In_{0.17}Ga_{0.83}As$	1.22	515
$In_{0.14}Ga_{0.86}As$	1.00	515

same stabilized substrate temperature.

High quality metamorphic $In_{0.14}Ga_{0.86}As$ virtual substrates, with a net compressive misfit over GaAs of 1.0%, have been achieved, as demonstrated by the TA-XRD (004) RSM of a 3-step metamorphic InGaAs structure given in Figure 3. As seen, the main diffraction peaks for each layer are strong and distinct with no significant mosaic spread that would otherwise suggest nonuniformity within a particular layer. Nearly full relaxation is obtained for all but the final step, as calculated from the XRD data and shown in the figure, indicating a highly controllable, slow increase in lattice constant in this metamorphic growth system. The outstanding bulk structural quality also yielded very regular surface crosshatch, as is

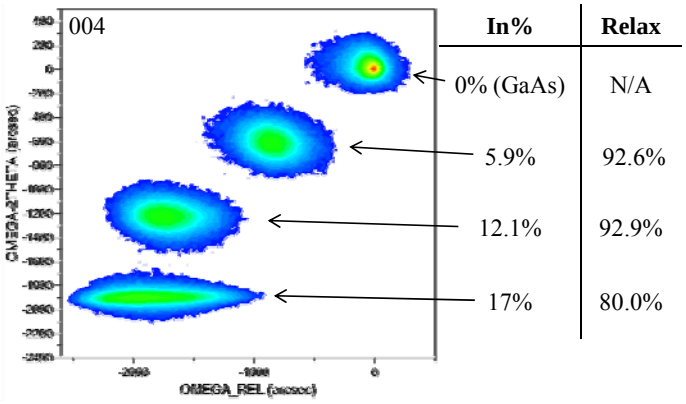

Figure 3. TA-XRD (004) RSM of a step-graded metamorphic $In_xGa_{1-x}As$ buffer structure grown on GaAs(100), accommodating a total 1% lattice misfit, from x = 0 (pure GaAs) to 0.17 ($In_{0.17}Ga_{0.83}As$), in three 0.5 µm thick steps (~0.4 % misfit per step). The layer compositions and magnitude of lattice relaxation calculated from this data is given.

desired for relaxation due to long misfit dislocation glide lengths at the internally mismatched interfaces.

The lack of full relaxation in the final step (in this particular case, $In_{0.17}Ga_{0.83}As$), due to insufficient strain energy to promote additional lattice relaxation by dislocation glide and/or nucleation, yields a final *effective* lateral lattice constant equal to that of fully-relaxed $In_{0.14}Ga_{0.86}As$. Because this is an intrinsic materials limitation in this system (and essentially all cation graded alloys), any final composition will exhibit such a lattice constant "undershoot." Therefore, in order to provide fully relaxed device layers, grown on the metamorphic InGaAs virtual substrate, a final effective lattice-matched $In_{0.14}Ga_{0.86}As$ "step-back layer" is grown on top of the incompletely relaxed $In_{0.17}Ga_{0.83}As$ layer. Subsequent device structures are then grown lattice-matched to the 14% In step-back layer, producing high quality, strain-free, low-dislocation density devices. Figure 4 displays a TA-XRD (224) RSM of such a metamorphic virtual substrate structure utilizing a 14% In step-back layer, with a final lattice-matched $In_{0.61}Ga_{0.39}P$ p-i-n detector structure grown on top.

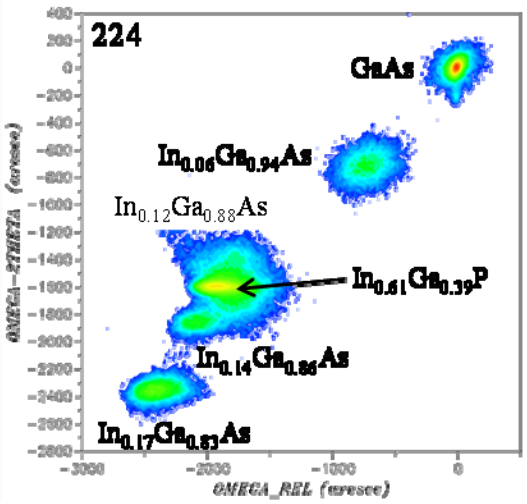

Figure 4. TA-XRD (224) RSM of a step-graded metamorphic $In_xGa_{1-x}As$ buffer, grown on GaAs(100), with a final $In_{0.14}Ga_{0.86}As$ step-back layer and lattice-matched $In_{0.61}Ga_{0.39}P$ p-i-n detector structure. Calculated layer compositions are given.

The resultant misfit dislocation (MD) network, with associated threading dislocation (TD) segments, at each interface was studied through TEM characterization of the graded buffer layers. It can be seen from Figure 5a, which shows a cross-sectional (X-TEM) view of the InGaAs step-graded buffer layers, that the majority of MDs (and their associated TDs) were created at the interface between the GaAs substrate and the $In_{0.06}Ga_{0.94}As$ layer. The goal of the InGaAs step-graded buffer is to reuse the TDs created early in the buffer (i.e. at the first misfit interface) to produce strain-relieving MD segments at each subsequent interface via glide at the strained interfaces, thereby minimizing the nucleation of new dislocations and keeping the total dislocation density to a minimum. Although this cannot be entirely

confirmed from Fig. 5a, it appears that there is no significant increase in the dislocation density in the subsequent InGaAs layers. The plan-view (PV-TEM) image in Fig. 5b shows no phase decomposition in

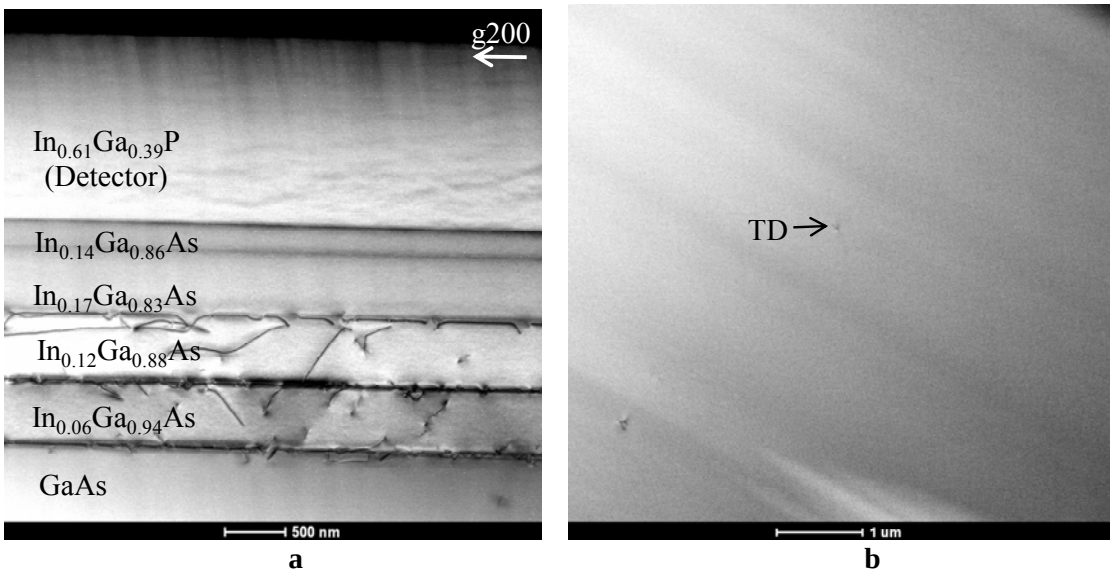

Figure 5. (a) X-TEM showing the InGaAs buffer layers along with the step-back $In_{0.14}Ga_{0.86}As$ and the final $In_{0.61}Ga_{0.39}P$ device layer. (b) Plan-view TEM showing the threading dislocations terminating at the surface. The images were obtained using g200 vector and [001] zone axis.

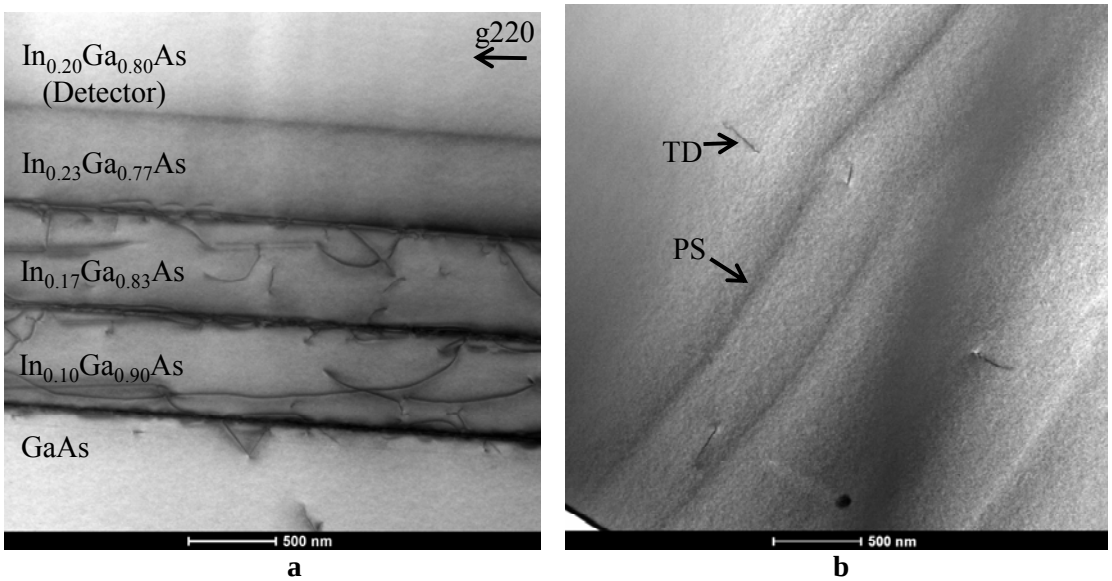

Figure 6. (a) Cross-sectional transmission electron micrographs showing the InGaAs buffer layers along with the very high quality $In_{0.20}Ga_{0.80}As$ device layer. (b) Plan-view TEM showing the threading dislocations terminating at the surface and the contrast lines due to phase segregation (PS). The images were obtained using g220 vector and [001] zone axis.

the terminal $In_{0.14}Ga_{0.86}As$ detector material, and indicates an average threading dislocation density (TDD) of ~5×10^6 cm^{-2}.

In order to access even longer IR wavelength cutoff, the metamorphic InGaAs buffer system was pushed out to even higher lattice constants. $In_{0.20}Ga_{0.80}As$ virtual substrates have been produced using a buffer structure of x = 0.10, 0.17, and 0.23, and a x = 0.20 step-back layer. As before, these layers are

almost completely relaxed and the peaks are strong, distinct and have reasonably low mosaic spread. TEM analysis of these metamorphic structures is shown in Figure 6. X-TEM (Fig. 6a) shows a dislocation evolution similar to that of the previous buffer. However, PV-TEM (Fig. 6b) shows lines of contrast, indicating a small degree of phase segregation, which has been previously reported for MBE-grown In compositions of greater than around 20%. The average threading dislocation density (TDD) calculated for these buffers ~1.5×10^{7} cm^{-2}. It should be possible to reduce TDD in this buffer by better optimizing the strain mitigation of the buffer design (e.g. adding another layer).

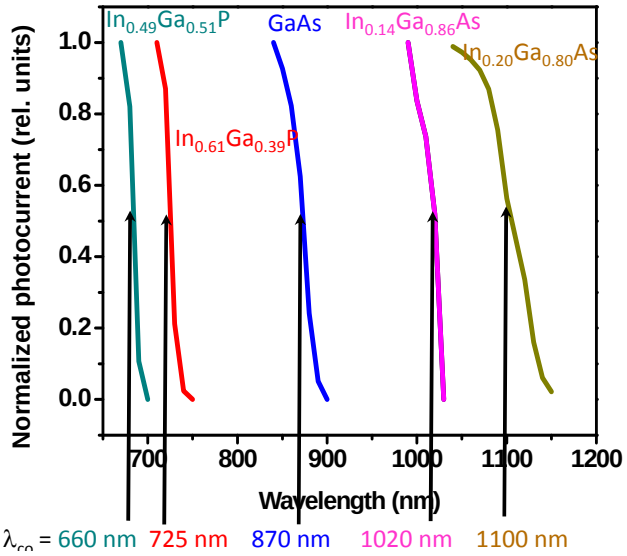

Figure 7. Near band-edge spectral response data measured for four different lattice-matched (GaAs and $In_{0.49}Ga_{0.51}P$) and metamorphic ($In_{0.14}Ga_{0.86}As$ and $In_{0.61}Ga_{0.39}P$) photodetector materials.

Using the different demonstrated InGaAs virtual substrates, as well as the GaAs substrate itself, a number of absorption profiles can be produced, as is a goal of this project. Figure 7 shows the near band-edge photoresponse measurements obtained for 5 different materials integrated on GaAs substrates: lattice-matched GaAs and $Ga_{0.51}In_{0.49}P$, and a number of metamorphic InGaAs and InGaP compositions, which utilize step-graded $In_xGa_{1-x}As$ buffers.

3.2. Metamorphic InGaAs near-IR photodetectors

The metamorphic $In_{0.14}Ga_{0.86}As$ and $In_{0.20}Ga_{0.80}As$ materials characterized in section 3.1 were grown into p-i-n structures and processed to form near-IR photodetectors with different cutoff wavelengths, ~1015 nm and ~1130 nm, respectively. P-i-n photodetectors with square active areas ranging from 50×50 μm^2 to 300×300 μm^2 were fabricated. Photolithography and inductively coupled plasma etching were used to define the mesa. Photo-definable polyimide was used to perform several functions, including planarization of the surface for front contact deposition, electrical isolation, and device sidewall passivation. Ni/Ge/Au and Cr/Au metal stacks were deposited using electron-beam evaporation to form n-type and p-type Ohmic contacts, respectively. No anti-reflection coating was applied. The cross-sectional image of a fabricated p-i-n $In_{0.20}Ga_{0.80}As$ photodetector is diagrammed in Figure 8.

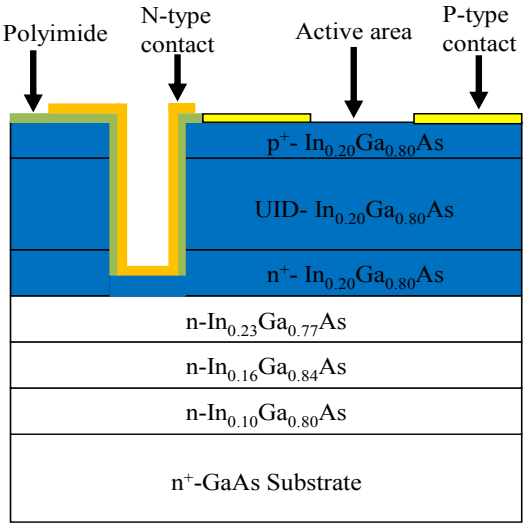

Figure 8. Cross-sectional view (not to scale) of a fabricated p-i-n $In_{0.20}Ga_{0.80}As$ photodetector. The $In_{0.64}Ga_{0.36}P$ window layer employed in actual devices is not shown.

The doped layer thicknesses for both detectors were designed to be 0.5 µm (5×10^{18} cm^{-3}, n-type) and 0.1 µm (5×10^{18} cm^{-3}, p-type). The unintentionally doped (UID) layer was 2.0 µm for the $In_{0.14}Ga_{0.86}As$ detector and 1.0 µm for the $In_{0.20}Ga_{0.80}As$ detectors. The growth was completed with 0.1 µm of window layer ($In_{0.61}Ga_{0.39}P$ for $In_{0.14}Ga_{0.86}As$ detector and $In_{0.64}Ga_{0.39}P$ for $In_{0.20}Ga_{0.80}As$ detector) to minimize loss due to surface recombination.

The presence of residual defects resulting from the necessary metamorphic strain relaxation can be an issue, and regardless of structural studies, it is electronic studies that allow us to verify the electronic quality and thus usefulness of these new types of materials for devices. Therefore, DLTS measurements were performed on the fabricated detector structures in order to evaluate the electronic quality of the intrinsic materials regions of the p-i-n devices by elucidating the nature and number of trap levels in the bandgap. The DLTS measurements on the $In_{0.14}Ga_{0.86}As$ detector structures, displayed in Figure 9, revealed very low total trap concentrations, $N_{T,tot}$, in the undoped device layers (which retain a slight n-type character due to background impurity levels) of $< 4\times10^{12}$ cm^{-3}, which compares quite favorably with that of lightly-doped n-GaAs (8×10^{12} cm^{-3}) and is an extraordinary result. The fact that the metamorphic samples possess equivalent or lower trap densities than their homoepitaxial counterpart prove that the metamorphic process, while resulting in a low residual threading dislocation density, do not contribute bandgap states that would have otherwise impacted ideal detector performance. It also shows that there are no significant point defect issues in these new classes of materials using our growth process, and thus they are of an appropriate quality for generating very high performance devices, and suggests very low noise and leakage levels, and thus an expectation of very high sensitivity even to low incident photon intensities; such properties were demonstrated, and are described below.

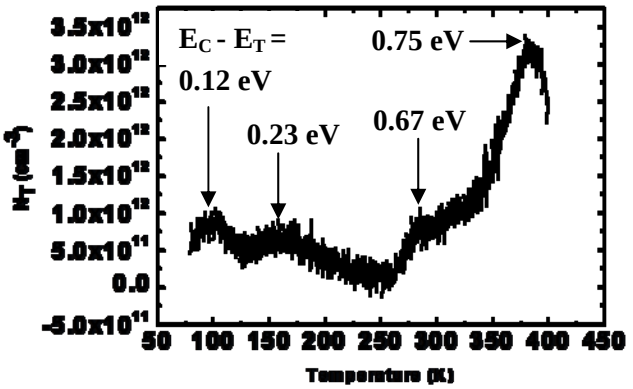

Figure 9. DLTS spectra for unintentionally doped metamorphic $In_{0.14}Ga_{0.86}As$, with the energy levels for each trap.

Dark current is an important figure of merit for a photodetector, which is directly related to the density and nature of traps in the bandgap. The lower the dark current, the better the signal-to-noise ratio, thus smaller absolute and relative signals can be detected. The dark current density versus bias voltage (J-V) plots for the $In_{0.14}Ga_{0.86}As$ and $In_{0.20}Ga_{0.80}As$ detectors are shown in Figure 10. As can be seen, both J-V's demonstrate good diode behavior with sharp forward-bias turn-on and an ideality factor between 1.6 (for $In_{0.14}Ga_{0.86}As$) and 1.2 (for $In_{0.20}Ga_{0.80}As$). This is combined with extremely low, room temperature reverse bias dark current density of $\sim1\times10^{-7}$ Acm^{-2} for $In_{0.14}Ga_{0.86}As$ and $\sim3\times10^{-7}$ Acm^{-2} for $In_{0.20}Ga_{0.80}As$ at -3V. In fact, the value obtained for the $In_{0.20}Ga_{0.80}As$ photodetector is orders of magnitude lower than

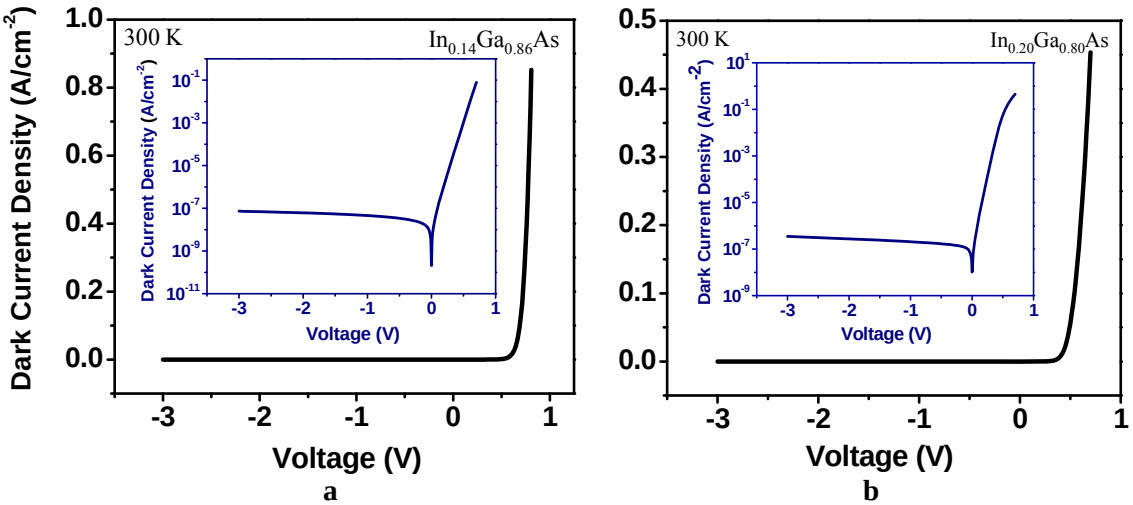

Figure 10. Room-temperature current density versus bias voltage measurements displaying very low reverse dark current for (a) $In_{0.14}Ga_{0.86}As$ detector and (b) $In_{0.20}Ga_{0.80}As$. The insets in the figures give the current density versus bias on a logarithmic scale.

that achieved for comparable back-illuminated InGaAs detectors found in the literature and is comparable to the commercially available $In_{0.53}Ga_{0.47}As$ p-i-n detectors grown lattice-matched to InP substrates (http://sales.hamamatsu.com/assets/pdf/parts_G/G8941_series.pdf). The slightly higher dark current density for the $In_{0.20}Ga_{0.80}As$ (1.1 eV) detector in comparison with that of the $In_{0.14}Ga_{0.86}As$ (1.22 eV) detector could be, at least partially, attributed to the narrower bandgap of the $In_{0.20}Ga_{0.80}As$ detector. It is likely that the ~2× increase in TDD and the slight phase segregation measured for $In_{0.20}Ga_{0.80}As$ has some impact on the detector performance, including a slight increase in the dark current of these detectors. That said, the net impact on device performance appears to be relatively small, and does not seem to significantly degrade the efficacy of the $In_{0.20}Ga_{0.80}As$ detectors. The full impact of such defects in these metamorphic materials on the detector performance is currently being investigated.

Responsivity profiles for the $In_{0.14}Ga_{0.86}As$ and $In_{0.20}Ga_{0.80}As$ detectors at room temperature, as a function of applied bias voltage (V_R) were measured and the results are presented in Figure 11. While the responsivity shows a sharp increase as soon as reverse bias is applied to the $In_{0.14}Ga_{0.86}As$ detector, there is only a small increase in responsivity with V_R for the $In_{0.20}Ga_{0.80}As$ detectors, which completely saturate at around -1V. This is due to the thinner (1.0 μm) intrinsic layer for the $In_{0.20}Ga_{0.80}As$ detectors, being already almost completely depleted under unbiased condition.

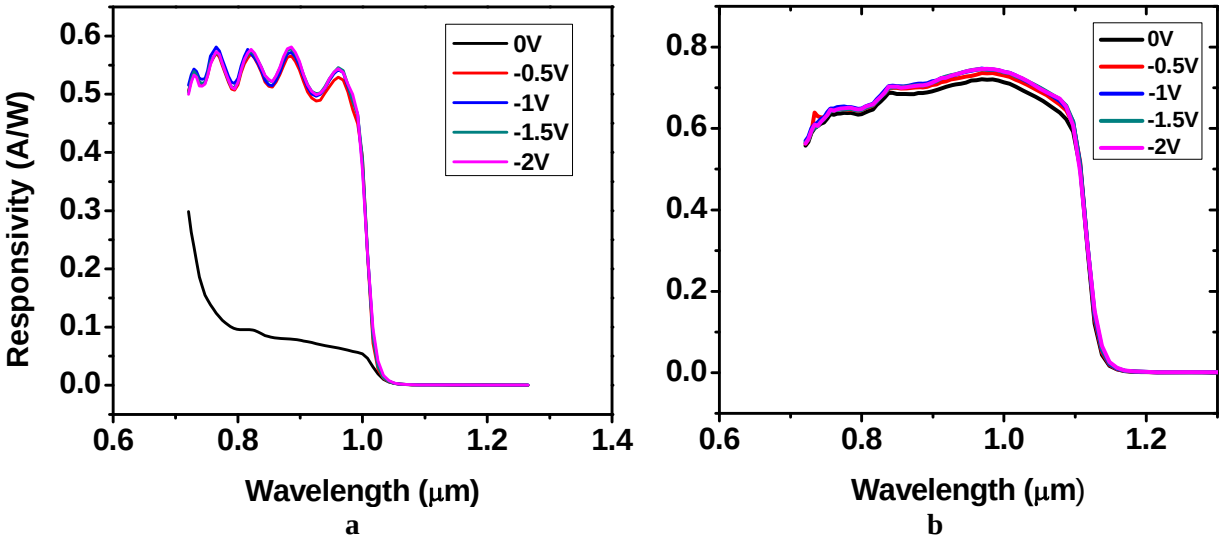

Figure 11. Spectral responsivity as a function of reverse bias voltage showing high responsivity for (a) $In_{0.14}Ga_{0.86}As$ and (b) $In_{0.20}Ga_{0.80}As$ detectors. The apparent interference fringing seen in (a) is most likely due to the thicker (2 μm) intrinsic region

Responsivity of the $In_{0.20}Ga_{0.80}As$ detector of 0.72 A/W achieved at 1030 nm is significantly higher than comparable commercial Si (0.55 A/W) and $In_{0.53}Ga_{0.47}As$ (0.64 A/W) p-i-n photodetectors (http://www.pacific-sensor.com/pages/sp_sq.html). Responsivity of 0.69 A/W at 1060 nm wavelength matches that achieved with the $In_{0.53}Ga_{0.47}As$ detector, but is much higher than the maximum value achieved with a Si detector (0.35 A/W). It should be noted that a thicker intrinsic layer could be used to further increase the responsivity for the $In_{0.20}Ga_{0.80}As$ due to the increased absorption of longer wavelength light. A significant improvement in the responsivity could also be achieved by the use of anti-reflection coating.

Another important figure of merit for a photodetector is the noise equivalent power (NEP). The shot noise dominated NEP is defined as I_n/R, the ratio of total noise current to responsivity at a particular wavelength and bias voltage. Low NEP values of 1.07×10^{-14} W/Hz$^{1/2}$ and 1.12×10^{-14} W/Hz$^{1/2}$ are achieved for 1030 nm and 1060 nm wavelengths respectively, at -2V. These values are comparable to commercial lattice-matched $In_{0.53}Ga_{0.47}As$ detectors that are grown on InP substrates.

The bandwidth of a p-i-n photodetector is determined by the RC time constant and the transit time for the photogenerated carriers. Although very low values for RC can be achieved for Si (which also

suffers from low R at wavelengths longer than 1030 nm), the need for thicker material to maximize responsivity results in very high transit times, limiting the cutoff frequency of these devices to a few MHz. In comparison, detectors with higher speeds on the order of a few GHz can be achieved with both metamorphic $In_{0.20}Ga_{0.80}As$ and $In_{0.53}Ga_{0.47}As$ mainly due to much shorter transit times. The metamorphic $In_{0.20}Ga_{0.80}As$ reported in this work was not optimized for high speed operation, and thus did not employ wider bandgap p- and n-doped layers to minimize the slow diffusion of carriers in the doped layers; such a materials adjustment is relatively straightforward to accomplish. However, even without these modifications, the capacitance and matching resistance measured at -2V were 8.55 pF and 60 Ω respectively. Assuming that the device is limited by the RC time constant (the transit time would be very small since the intrinsic layer is only 1.0 μm), we calculate a theoretical 3-dB bandwidth of 3.1×10^8 Hz and a bandwidth-responsivity product of 0.21 GHz.A/W at 1060 nm, impressive values that again point to the technology game-changing capability of this early stage prototype.

3.3. Lattice-matched and metamorphic InGaP visible photodetectors

With the IR band materials and single junction detector prototypes established, we then turned to the shorter wavelength sub-detector materials and devices. These were first developed as single-band visible detectors at the same lattice constants as the InGaAs IR detectors, prior to their integration into a multiband design, as described in the next section. $In_{0.49}Ga_{0.51}P$ grown lattice-matched to GaAs substrates and $In_{0.61}Ga_{0.39}P$ grown lattice-matched to the $In_{0.14}Ga_{0.86}As$ virtual substrate were fabricated into p-i-n visible wavelength photodetectors with different cut-off wavelengths, using a structure and fabrication process similar to that described for the InGaAs detectors. A quaternary AlGaInP window layer was grown lattice matched to the InGaP device layers to reduce surface recombination.

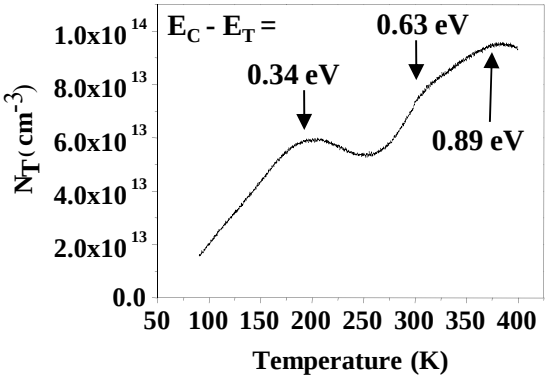

Figure 12. DLTS spectrum for unintentionally doped metamorphic $Ga_{0.39}In_{0.61}P$, with the energy levels for each trap as shown.

As with the metamorphic InGaAs detectors, DLTS measurements were also performed on the metamorphic $In_{0.61}Ga_{0.49}P$ photodetector structures. These measurements, displayed in Figure 12, also revealed very low total trap concentrations of $<1\times10^{14}$ cm^{-3}, which compares favorably with that of a lightly-doped n-$Ga_{0.51}In_{0.49}P$ lattice-matched to GaAs (3×10^{14} cm^{-3}). Note that the higher trap density for InGaP samples versus (In)GaAs is typical for InGaP materials due to its wider bandgap and the small, unavoidable oxygen contamination from the phosphorus cracker source. And again, as with the InGaAs samples, the fact that the metamorphic samples possess equivalent or lower trap densities than their lattice-matched counterpart prove that the metamorphic nature of these materials does not contribute additional bandgap states.

Outstanding results were obtained from our prototype lattice matched and metamorphic single junction InGaP detectors. Figure 13a displays the current density versus applied bias (J-V) characteristics of a lattice matched (LM) $In_{0.49}Ga_{0.51}P$ prototype photodetector measured in the dark. The very high material quality is confirmed in the final device by the excellent forward bias characteristics and ultra-low, voltage independent reverse dark current density ($<1\times10^{-12}$ Acm^{-2}), below even the detection limit of the high-resolution electrometer used for the measurement. In fact, a careful perusal of the existing literature shows that the leakage currents we have achieved are, to our knowledge, by far the lowest reported for any InGaP based detector.

The dark J-V characteristics of the metamorphic $In_{0.61}Ga_{0.39}P$ are shown in Figure 13b. The higher reverse current in comparison with the LM-InGaP detector could be due to a combination of reasons. A somewhat higher dark current is expected due to the lower bandgap of the $In_{0.61}Ga_{0.39}P$ detector (1.7 eV) compared to the LM-InGaP detector (1.9 eV). However, this is likely due to the

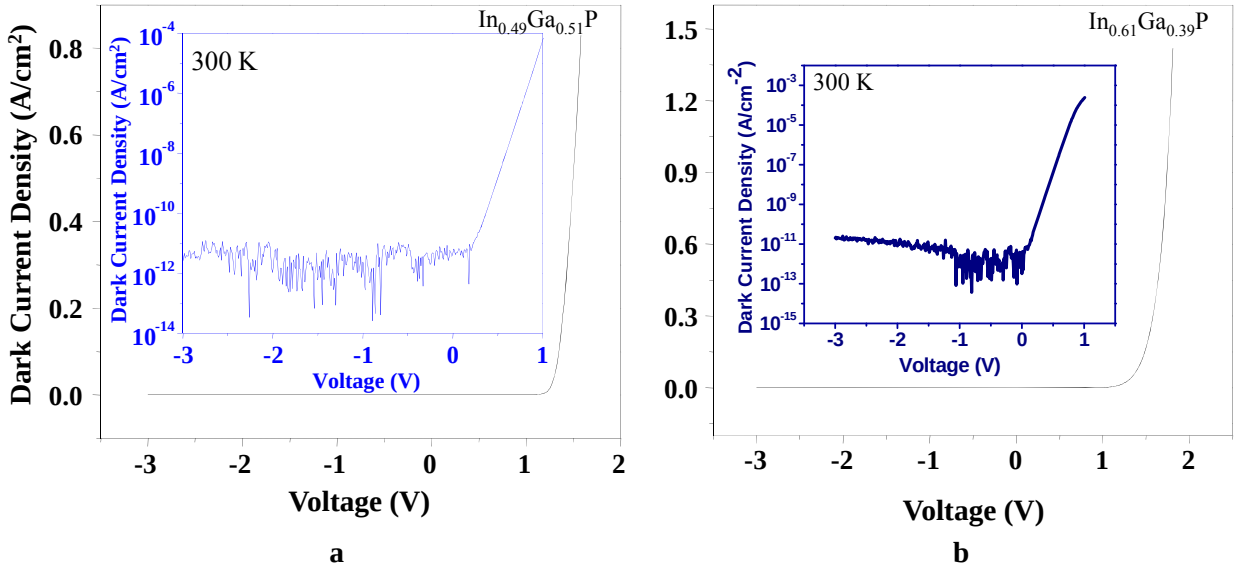

Figure 13. Room-temperature current density versus bias measurement of the (a) $In_{0.49}Ga_{0.51}P$ and (b) $In_{0.61}Ga_{0.39}P$ p-i-n photodetector structures, displaying very low reverse current. If fact, the leakage current for the lattice-matched detectors is below our electrometer detection limit. The insets in both figures give the current density versus bias on a logarithmic scale.

presence of threading dislocations in the metamorphic structure. Nonetheless, the extremely low value of the dark current density for these MM-$In_{0.61}Ga_{0.39}P$ detectors implies that we can expect very good device performance.

Metamorphic $In_{0.61}Ga_{0.39}P$ photodetectors grown on GaAs substrates could perform as ideal infrared-blind visible detectors that are important for many applications due to their direct bandgap of around 1.7 eV (cutoff wavelength ~730 nm) and potential for high speed and high responsivity. Responsivity as a function of wavelength for the MM-$In_{0.61}Ga_{0.39}P$ photodetectors is shown in Figure 14. A very high responsivity value of 0.38A/W is achieved at 680 nm wavelength.

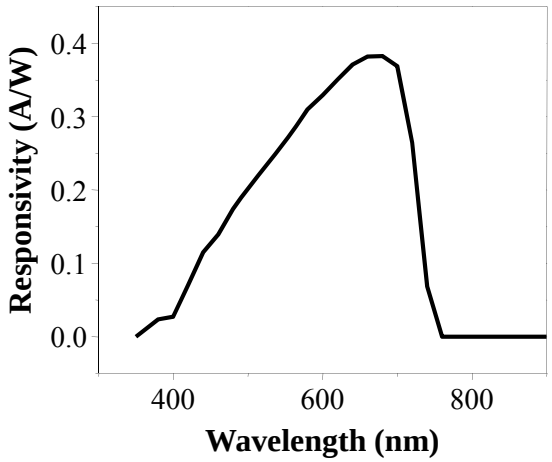

Figure 14. Responsivity as a function of wavelength at 0V, showing high responsivity for the $In_{0.61}Ga_{0.39}P$ photodetectors.

3.4. Monolithic vertically-integrated lattice matched and metamorphic visible/near-IR dual-band detector design and fabrication

Having developed and demonstrated high-quality InGaAs (near-IR) and InGaP (visible) single detector structures integrated with metamorphic InGaAs virtual substrates at identical lattice constants, we then worked on the development of a mutli-spectral detector architecture. In our approach, we stack the detectors in a manner similar to that of multijunction solar cells, with the high bandgap sub-detector on top and the low bandgap sub-detector below, allowing for top-side illumination. In order to allow for independent electrical addressing of the integrated sub-detectors and simultaneous detection without need for active control, we developed a three-terminal back-to-back p-i-n diode structure, with a common p-type contact in the middle. These dual-detectors are thus designed to operate simultaneously and independently in the visible/near-IR wavelengths, with acceptably low optical crosstalk and complete electrical isolation between sub-detectors. Prototype LM-GaAs/$In_{0.49}Ga_{0.51}P$ and MM-

$In_{0.14}Ga_{0.86}As/In_{0.61}Ga_{0.39}P$ dual-detector n-i-p/p-i-n structures were grown and fabricated for testing and comparison.

Figure 15 provides a diagrammatic cross-sectional view of the fabricated n-i-p/p-i-n $In_{0.14}Ga_{0.86}As/In_{0.61}Ga_{0.39}P$ visible/IR 2-band device structure. The simulated corresponding energy-band diagram (calculated using ATLAS TCAD device simulation software from Silvaco) at thermal equilibrium and the direction of carrier flow in each sub-detector are shown in Figure 16. This clearly indicates how the use of a back-to-back n-i-p/p-i-n diode structure allows for the isolation and measurement of currents generated by each sub-detector. In order to prevent leakage of photogenerated electrons from the p-InGaP layer into the InGaAs device (electro-optical cross-talk), and large bandgap AlGaInP back surface field (i.e. charge reflector) layer is placed in between the two diodes.

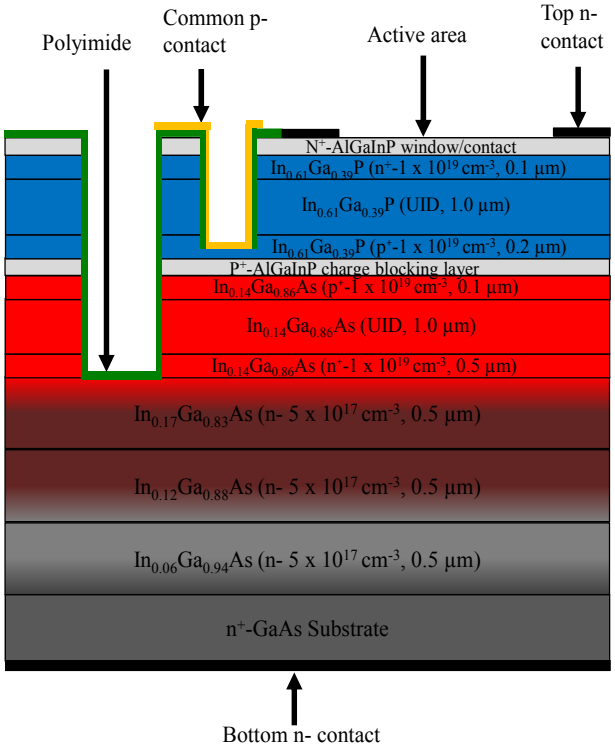

Figure 15. Cross-sectional view (not to scale) of a fabricated n-i-p/p-i-n $In_{0.61}Ga_{0.39}P/In_{0.14}Ga_{0.86}As$ dual-photodetector with AlGaInP window and BSF (charge blocking) layers.

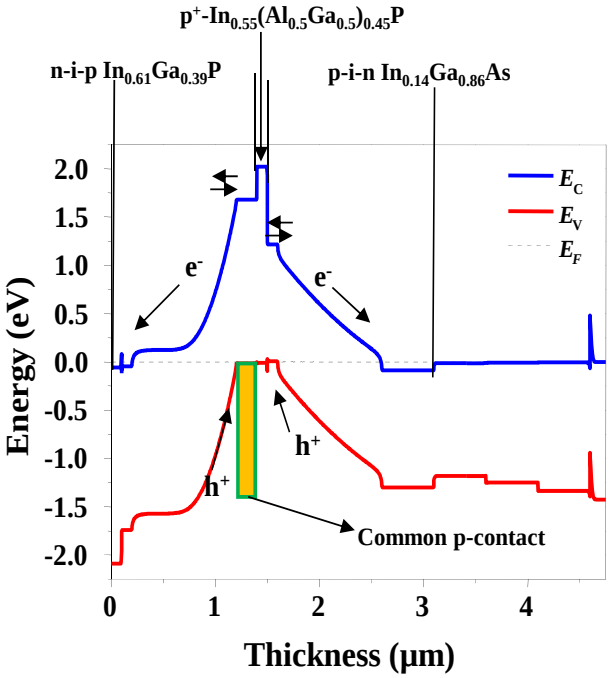

Figure 16. Simulation of the energy band-diagram at thermal equilibrium for the n-i-p/p-i-n $In_{0.61}Ga_{0.39}P/In_{0.14}Ga_{0.86}As$ dual-photodetector structure with AlGaInP window and BSF layers.

3.5. LM and MM dual-photodetector characterization

The electrical isolation between the sub-detectors was studied by measuring the dark current densities of both sub-detectors as a function of bias voltage applied to each sub-detector, independently. It can be seen from the dark J-V plot shown in Figure 17a that when a reverse bias is applied to the $In_{0.61}Ga_{0.39}P$ sub-detector there is no change in the dark current of the $In_{0.14}Ga_{0.86}As$ sub-detector, and there is only a slight increase in reverse dark current for the $In_{0.61}Ga_{0.39}P$ sub-detector. Under forward bias condition, the $In_{0.61}Ga_{0.39}P$ sub-detector turns on as expected, with a sharp increase in forward current. The corresponding measurement for the $In_{0.14}Ga_{0.86}As$ sub-detector does show an increase in the negative current. This initially unexpected result turns out to be due to the generation of photons in the $In_{0.61}Ga_{0.39}P$ sub-detector (i.e. acting as an LED), which are then detected by the $In_{0.14}Ga_{0.86}As$ sub-

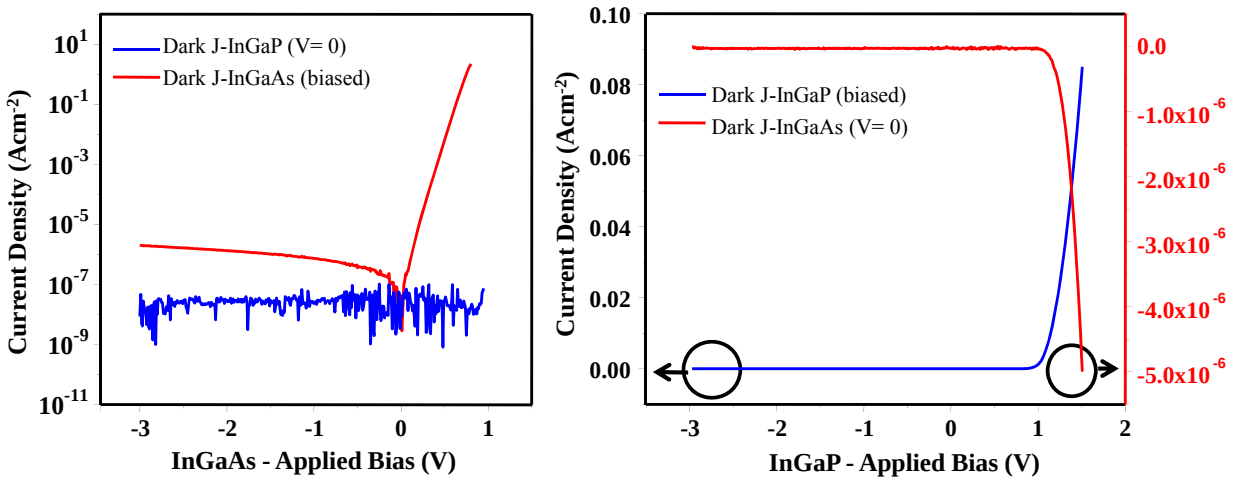

Figure 17. Dark J-V for both $In_{0.61}Ga_{0.39}P$ and $In_{0.14}Ga_{0.86}As$ sub-detectors as a function of applied bias voltage to each sub-detector.

detector. The dark J-V when reverse bias voltage applied to the $In_{0.14}Ga_{0.86}As$ sub-detector (see Fig. 17b) shows similar behavior as in Fig 17a. However, there is no increase in negative current for the $In_{0.61}Ga_{0.39}P$ sub-detector under forward bias to the $In_{0.14}Ga_{0.86}As$ sub-detector, any light emitted by the $In_{0.14}Ga_{0.86}As$ sub-detector is lower energy than the bandgap of $In_{0.61}Ga_{0.39}P$. Despite the LED effect, these result indicate that there is indeed complete electrical isolation between the sub-detectors achieved using the n-i-p/p-i-n structure. These plots also show that that these dual-detectors could potentially also work as monolithic dual-LEDs under forward bias condition for both sub-detectors. Similar behavior was observed with LM-dual detectors.

Normalized EQE profiles measured simultaneously for both sub-detectors in the LM- and MM-dual-detector devices, at room temperature, zero applied bias, and over the wavelength range of 350 nm to 1100 nm are presented in Figure 18. No anti-reflection layers were applied to the devices. The cutoff wavelengths of the $In_{0.14}Ga_{0.86}As$ (1020 nm) and $In_{0.61}Ga_{0.39}P$ (725 nm) detectors correspond to their respective band-gaps of 1.2 eV for $In_{0.14}Ga_{0.86}As$ and 1.7 eV for $In_{0.61}Ga_{0.39}P$, as measured using room temperature photoluminescence. It can be observed that there is very little optical crosstalk between the

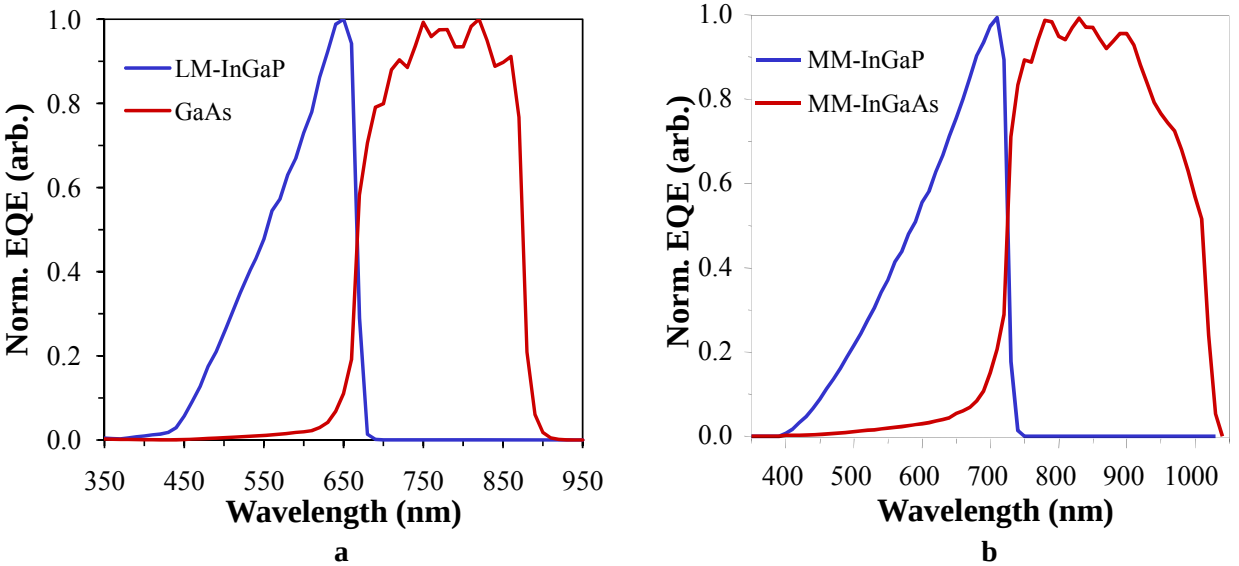

Figure 18. Normalize EQE as a function of wavelength showing very low optical cross-talk between sub-detectors for (a) LM-dual detectors and (b) MM-dual detectors.

sub-detectors except for an overlap in the wavelength range of 700-730 nm for the metamorphic dual-detector structure. This is mainly due to the transmission of photons through the $In_{0.61}Ga_{0.39}P$ device layers and the consequent absorption by the $In_{0.14}Ga_{0.86}As$ layers. The crosstalk is higher for photons with energy at and just above the bandgap of the $In_{0.61}Ga_{0.39}P$ device layers due to the lower near-E_g absorption coefficient. This effect can be minimized by using thicker $In_{0.61}Ga_{0.39}P$ layers or by growing a notch filter layer to cut out that narrow band of overlap between the two sub-detector elements. Optical responsivities and external quantum efficiencies are expected to increase by about 30% when anti-reflection coating is applied, as well.

Perhaps the most important technology result here is that the two InGaAs and InGaP sub-detectors, which perform better than equivalent commercially available devices in single-detector format, perform equally as well within the vertically-integrated monolithic dual-detector structure as they do when they are grown in single-detector format, thanks to both the high level of materials quality achieved and the use of an innovative back-to-back diode configuration. Such a result provides a clear demonstration of the game-changing success of our metamorphic materials approach for the achievement of the project goal of developing a materials platform technology for the production of tunable, mission-optimized multispectral photodetectors. Ongoing work to extend the range of achievable terminal lattice constants, in concert with further optimization of the metamorphic buffer designs, will expand the number and variety of available detection bands while maintaining high materials quality, allowing for the continued production of high-performance, high-sensitivity multispectral photodetectors for use in any number of important applications.

4. Demographics During Project Period

Researchers Supported or Partially Supported	Status
Krishna Swaminathan	PhD Candidate (degree expected 2012)
Dr. Tyler Grassman	Postdoc (completion expected 2011)
Matthew Lueck	MS received 2008 (Research Triangle Institute)
Yong Lin	PhD received 2009 (NREL)

5. Publications with Synopses

This project has supported or partially supported 8 journal publications accepted or in print to date, 2 that are currently submitted and in review, and 1 additional paper in preparation. Additionally, the project has supported or partially supported 14 conference proceedings and presentations, of which 6 were invited. The list does not include invited colloquia and seminars given at various universities, government labs and industry.

List of AFOSR-supported journal publications grouped by subject matter:

A. Complex III-V interfaces, defects and epitaxy control for advanced detector epitaxy

This set of journal publications focused on perfecting the MBE-grown interfaces between dissimilar materials as a function of increasing dissimilarity, e.g. chemical compositions, lattice constants, crystal structure and heterovalency. The cumulative effects and impact of this work was to establish the basic understanding of defect mitigation during the formation of interfaces with monolayer control. Key findings were the establishment of Al(Ga)InP/GaAs interface stability as a function of temperature at the local (nm) scale, and the demonstration that 2-D defects due to chemically-driven interface nucleation events, such as stacking faults and antiphase domains, could be controlled and eliminated by appropriate

epitaxy initiation conditions and surface vicinality. Additionally, it was demonstrated that the GaAsP system of materials can enable a high degree of strain relaxation while maintaining control of dislocation nucleation rates, leading to low dislocation density material platforms that can support visible and near IR detector combinations, starting either with a "transparent" GaP or large area Si substrate, both of which enable a path toward high degrees of integratable detector structures, including with ROICs.

- P. Smith, M. Lueck, S.A. Ringel, and L.J. Brillson, "Atomic diffusion and electronic structure in $Al_{0.52}In_{0.48}P$/GaAs heterostructures," *J. Vac. Sci. Tech. B* ***25***, pp. 1916 – 1921 (2007).
- P.E. Smith, M. Lueck, S.A. Ringel, and L.J. Brillson, "Atomic Diffusion and Interface Electronic Structure at $In_{0.49}Ga_{0.51}P$/GaAs Heterojunctions," *J. Vac. Sci. Technol. B* ***26***, pp. 89-95 (2008).
- T. J. Grassman, M. R. Brenner, S. Rajagopalan, R. R. Unocic, R. R. Dehoff, M. J. Mills, H. L. Fraser, S. A. Ringel, "Control and elimination of nucleation-related defects in GaP/Si(001) heteroepitaxy," *Appl. Phys. Lett.* ***94***, 232106 (2009).
- T. J. Grassman, M. R. Brenner, M. Gonzalez, A. M. Carlin, R. R. Unocic, R. R. Dehoff, M. J. Mills, S. A. Ringel, "Characterization of metamorphic GaAsP/Si materials and devices for photovoltaic applications," *IEEE Trans. Electron Dev.* ***57***, 3361 (2010).

B. Metamorphic III-V materials for advanced detector heterostructures: structural, optical and electronic properties

This set of journal papers revealed the first demonstration of optimum graded anion buffers by MBE, the first comprehensive explanation of strain relaxation properties in this promising type of metamorphic buffer, and were used to demonstrate the first characterization of bulk versus surface transport properties of InAs materials. Additionally, it was shown that high-quality heterojunction IR devices with lattice constants that can only be achieved via metamorphic virtual substrate technology, here a TPV device having a wavelength cutoff of 2 μm, can be fabricated with unprecedented performance due to the ability to keep defect densities low. It was also shown that the span of bandgaps captured by lattice constants between InP and InAs can now be used for device, and specifically detector, applications.

- Y. Lin, A. Arehart, A. M. Carlin, and S. A. Ringel, "Separation of bulk and surface electron transport in metamorphic InAs layers using quantitative mobility spectrum analysis," *Appl. Phys. Lett.* ***93***, 062109 (2008).
- M. K. Hudait, Y. Lin, and S. A. Ringel, "Strain relaxation properties of $InAs_yP_{1-y}$ metamorphic materials grown on InP substrates," *J. Appl. Phys.****105***, 061643 (2009).
- M. K. Hudait, M. R. Brenner and S. A. Ringel, "Metamorphic $In_{0.7}Al_{0.3}As/In_{0.69}Ga_{0.31}As$ Thermophotovoltaic Devices Grown on Graded $InAs_yP_{1-y}$ buffers by Molecular Beam Epitaxy," *Solid State Electron.* ***53***, 102 (2009).

C. Detector heterostructures, materials characterization and devices

This set of journal papers was built upon findings from the above work, culminating with reports of the first high performance p-i-n metamorphic InGaAs and InGaP detectors with multiple cutoff wavelengths in several near IR and visible bands, and demonstrations that such devices outperform both commercial Si and literature-reported detectors in similar wavelength ranges, in spite of being lattice mismatched. Wavelength cutoffs from ~0.65 μm to 1.1 μm were demonstrated on the same metamorphic substrate platform. A unique back-to-back 3-terminal 2-color vertically integrated detector design was conceived, grown, fabricated and demonstrated, in which both visible and IR bands can be simultaneously detected, with no need for active bias control to achieve complete electrical isolation, and which display near total

optical out-of-band rejection. The performance of the sub-detectors were shown to be state-of-the-art in this format, which establishes this unique device concept as a realistic path for future, vertically integrated multi-color detectors that avoid both the need for bulky external optical control and the need for external bias control for band discrimination. The details of the technical report primarily focused on this topic as the papers are in review currently, with one more in preparation.

- M. González, and A. M. Carlin, C. Dorhman, E. A. Fitzgerald, and S. A. Ringel, "Determination of bandgap states in p-type $In_{0.49}Ga_{0.51}P$ grown on SiGe/Si and GaAs by deep level optical spectroscopy and deep level transient spectroscopy," *J. Appl. Phys.*, accepted for publication (2010).
- K. Swaminathan, L. Yang, T. J. Grassman, G. Taberas, A. Hierro, and S. A. Ringel, "Metamorphic $In_{0.20}Ga_{0.80}As$ p-i-n photodetectors grown on GaAs substrates for near infrared applications," *Optics Express*, submitted (2010). [contents summarized earlier in report]
- K. Swaminathan, T. J. Grassman, and S. A. Ringel, "Monolithically and vertically integrated visible-near infrared metamorphic dual-photodetectors grown on GaAs substrates," *J. Appl. Phys.*, submitted (2010). [contents summarized earlier in report]
- K. Swaminathan, T. J. Grassman, and S.A. Ringel, "Compressive Overshoot and Stepback for Optimized Metamorphic InGaAs Growth and Device Applications by Molecular Beam Epitaxy," *J. Appl. Phys.*, in preparation (2010). [contents summarized earlier in report]

List of AFOSR-supported conference presentations and proceedings (*denotes invited):

- A. M. Carlin, Y. Lin, M. R. Brenner, J. Boeckl, and S. A. Ringel, "Investigations of Anion Sublattice Grading in Quaternary Metamorphic GaInAsP Buffers Grown on GaAs," presented at the *50th TMS/IEEE Electronic Materials Conf.*, Santa Barbara, CA, June 2008.
- *S. A. Ringel, T. J. Grassman, and M. J. Brenner, "Advances in Defect Control for High Performance Metamorphic III-V devices," *International Conference on Electronic Materials (ICEM) and International Union of Materials Research Society (IUMRS)*, Sydney Australia (2008).
- S. A. Ringel, T. J. Grassman, M. J. Brenner, and J. Park, "Monolayer-Engineered Heterovalent GaP/Si Interfaces and Comparison with GaAs/Ge by Molecular Beam Epitaxy," *International MRS AAA Meeting*, Beijing, China (2008).
- T. J. Grassman, M. R. Brenner, A. M. Carlin, S. Rajagopalan, H. L. Fraser, J. Boeckl, and S. A. Ringel, "Metamorphic GaAsP ~1.7 eV Solar Cell Materials and Structures Grown on Si Substrates using Anion-Graded $GaAs_yP_{1-y}$ Buffers," presented at the *Fall Materials Research Society Meeting*, Boston, MA, December 2008.
- *S. A. Ringel, "GaAsP on Si heteroepitaxy for III-V/Si integration," *WOCSEMMAD*, Ft. Myers, FL (2009).
- T. J. Grassman, M. R. Brenner, A. M. Carlin, S. Rajagopalan, R. R. Unocic, R. R. Dehoff, M. J. Mills, H. L. Fraser, and S. A. Ringel, "Toward metamorphic multijunction GaAsP/Si photovoltaics grown on optimized GaP/Si virtual substrates using anion-graded $GaAs_yP_{1-y}$ buffers," *Proc. 34th IEEE Photovoltaic Specialists Conf.*, 002016 (2009).
- K. Swaminathan, T. J. Grassman, Q. Gu, T. Homan, and S.A. Ringel, "Metamorphic InGaAs and InGaP on GaAs for Multispectral detector applications," presented at the *51st TMS/IEEE Electronic Materials Conf.,* State College, PA, June 2009.
- *S. A. Ringel, T. J. Grassman, M. R. Brenner, R. Unocic, R. Dehoff, and M. Mills, "Solar cells using metamorphic substrates," *WOCSDICE*, Malaga, Spain (2009).
- T. J. Grassman, M. R. Brenner, A. M. Carlin, S. Rajagopalan, R. R. Unocic, R. R. Dehoff, M. J. Mills, H. L. Fraser, and S. A. Ringel, "Toward Metamorphic Multijunction GaAsP/Si Photovoltaics Grown on Optimized GaP/Si Virtual Substrates using Anion-Graded $GaAs_yP_{1-y}$ Buffers," presented at the *51st TMS/IEEE Electronic Materials Conference*, State College, PA, June 2009.

- *S. A. Ringel, “III-V/Si Heterointegration for Photovoltaics,” *216th Electrochechemical Society Meeting*, Vienna, Austria (2009).
- *S. A. Ringel, “The impact and control of defects in metamorphic III-V heterostructures," *13th International Conference on Defects - Recognition, Imaging and Physics in Semiconductors (DRIP XIII)*, Wheeling, WV (2009).
- T. J. Grassman, M. R. Brenner, A. M. Carlin, S. Rajagopalan, R. R. Unocic, R. R. Dehoff, M. J. Mills, H. L. Fraser, and S. A. Ringel, “Toward Metamorphic Multijunction GaAsP/Si Photovoltaics Grown on Optimized GaP/Si Virtual Substrates using Anion-Graded $GaAs_yP_{1-y}$ Buffers,” presented at the *36th IEEE International Symposium on Compound Semiconductors*, Santa Barbara, CA, August 2009.
- *S. A. Ringel and T. J. Grassman, “Defect Engineering in III-V/Si Photovoltaic Materials Based on GaP/Si Interfaces,” *Spring 2010 Meeting of the Materials Research Society*, San Francisco, CA (2010).
- T. J. Grassman, A. M. Carlin, and S. A. Ringel, “Metamorphic GaAsP and InGaP photovoltaic materials on Si for high-efficiency III-V/Si multijunction solar cells,” *Proc.35th IEEE Photovoltaic Specialists Conf.*, 002029 (2010).